# Theoretical Studies of Alkyl Radicals in the NaY and HY Zeolites

## Khashayar Ghandi,*,[†] Federico E. Zahariev,[‡] and Yan Alexander Wang[‡]

*Department of Chemistry, Mount Allison University, Barclay Building, 63C York Street, Sackville, NB, Canada E4L 1G8, and Department of Chemistry, University of British Columbia, Vancouver, B.C., Canada V6T 1Z1*

*Received: April 8, 2005; In Final Form: June 16, 2005*

Interplay of quantum mechanical calculations and experimental data on hyperfine coupling constants of ethyl radical in zeolites at several temperatures was engaged to study the geometries and binding energies and to predict the temperature dependence of hyperfine splitting of a series of alkyl radicals in zeolites for the first time. The main focus is on the hyperfine interaction of alkyl radicals in the NaY and HY zeolites. The hyperfine splitting for neutral free radicals and free radical cations is predicted for different zeolite environments. This information can be used to establish the nature of the muoniated alkyl radicals in the NaY and HY zeolites via $\mu$SR experiments. The muon hyperfine coupling constants of the ethane radical cation in these zeolites are very large with relatively little dependence on temperature. It was found that the *intramolecular* dynamics of alkyl free radicals are only *weakly affected* by their strong binding to zeolites. In contrast, the substrate binding has a *significant effect* on their *intermolecular* dynamics.

## Introduction

Zeolites, alumino-hydro-silicates with pores of molecular dimensions, are catalysts widely used in hydrocarbon transformations,[1] the methanol-to-gasoline process,[2] and polymer synthesis.[3] The largest gap in our knowledge of such processes is microscopic information about organic radical intermediates in zeolites.

The wide range of catalytic reactions that may involve H atoms absorbed on the surface[2,4−7] led to the proposed facilitation of neutral free radical formation by H-addition reactions.[8] The muon spin rotation ($\mu$SR) study of muoniated free radicals has been found to be essential to identify free radical binding sites in catalysts, particularly zeolites.[9−13] Indeed, the first observation of a complex involving a neutral organic free radical and a diamagnetic metal ion in zeolites was through $\mu$SR.[10] Similarly, for the first time the changes in molecular geometry of a free radical due to interaction with the zeolite extraframework cations were reported.[12b] The valuable information that could be gained by comparison of predictions of quantum mechanical calculations and $\mu$SR studies motivates the current work where we seek to understand the role of guest−host interactions in determining structures, vibrational frequencies, isotropic hyperfine coupling constants, and reactivity of alkyl radicals in the NaY and HY zeolites.

This paper contains five sections. In the next section, the methods will be introduced. The available experimental data are limited to ethyl radicals in the NaY zeolite (at a loading of one per supercage), and will be used to evaluate our computational strategy in the third section. In the third section, we will discuss our results of methyl, ethyl, and *tert*-butyl radicals in the NaY and HY zeolites. We will use theoretical calculations to predict the binding sites of alkyl radicals in the HY zeolite and the trend of binding of alkyl radicals in the NaY and HY zeolites. We will focus on hyperfine interactions of the ethyl

radical in zeolites. Of particular importance are hyperconjugation of the unpaired electron from the methylene $\alpha$ position onto the $\beta$ methyl group hydrogen and the direct dipolar interactions of $\beta$ protons with the unpaired electron.

The $\mu$SR technique and its application in free radical chemistry have been well documented elsewhere.[14−15] The radicals studied by the $\mu$SR technique are mostly formed from addition of muonium (Mu) to a double bond.[9−15] Mu is an ultralight isotope of hydrogen with 1/9 the mass of H (1/18 the mass of D). The large mass ratio of H/Mu causes the muon hyperfine coupling constant in muoniated alkyl radicals to vary dramatically with temperature,[14,15] unlike the alkyl radical's proton hyperfine coupling constant typically measured by ESR.[16,17]

Two methods are usually used to characterize the muoniated free radicals in zeolites.[9−13] In the Transverse Field-$\mu$SR (TF-$\mu$SR),[14] the precession of the muon spin polarization in a transverse magnetic field at frequencies corresponding to the allowed transitions between energy levels of the spin Hamiltonian of muoniated radical is the observable.

In polycrystalline environments, such as zeolites, the frequencies can be modified by the average over the angular dependence of the dipolar coupling.[10]

The Avoided Level Crossing-$\mu$SR (ALC-$\mu$SR)[14] is the other method that has been used to characterize the muoniated free radicals in zeolites.[9−13] There are usually two different types of ALC resonance corresponding to the magnetic selection rules characterized by $\Delta M = \Delta(m_e + m_\mu + m_k)$, where $\mu$ stands for muon, e for electron, and k another spin bearing nucleus (e.g., H nucleus), and $m_i$ is the magnetic quantum number of particle i. The $\Delta M = 0$ resonance arises from isotropic couplings in the spin Hamiltonian.[14] This is the only kind of ALC resonance expected when the dipolar couplings are averaged to zero by fast rotational tumbling. The other ALC resonance, $\Delta M = 1$ transition, is induced by coupling of Zeeman states directly from the anisotropic part of the muon hyperfine interaction.[14]

A key question that each experiment deals with is the assignment of the observed spectra to corresponding free

---

[†] Mount Allison University.
[‡] University of British Columbia.

Alkyl Radicals in Zeolites

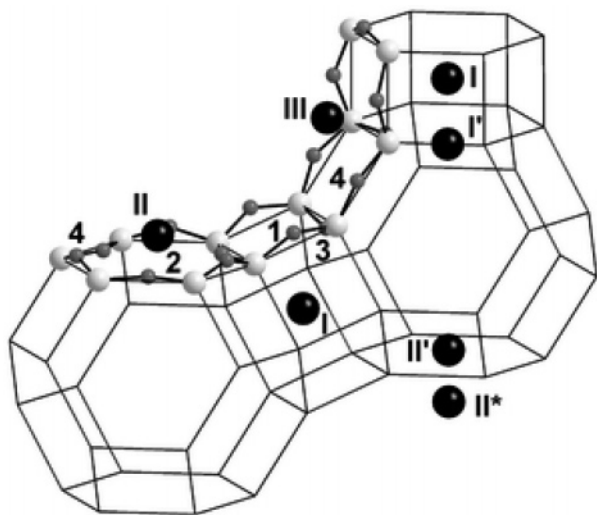*J. Phys. Chem. A, Vol. 109, No. 32, 2005* **7243**



**Figure 1.** Different cation sites in Y zeolites (adapted from ref 32 with permission).

radicals: Are the formed free radicals ionic or neutral? Where are the binding sites for different free radicals? Unambiguous assignment is achieved by comparison with computational predictions.

In the following sections, after the computational methods are introduced, the effect of guest−host interactions on the structures, binding strengths, and energies of free radicals will be discussed. Then, the effect of guest−host interactions on internal hindered rotations, vibrations, and different conformations as a function of the temperature will be discussed. Finally, a series of theoretical predictions will be outlined to pave the way for future experiments.

**Method**

Calculations in the absence of zeolite framework were carried out with the Gaussian-98 program.[18] The B3LYP/6-31G(d,p) method [19−24] was used to optimize geometries; while the B3LYP/6-311+G (2df,p) method [25] was used to calculate hfcs and spin densities.

For calculations in the presence of the zeolite framework, a two-layered ONIOM model was employed.[25−30] In this model, the B3LYP hybrid density functional is used for the host−radical complexes with $H^+$ or $Na^+$ (the first layer) and the Hartree−Fock method for the zeolite framework (the second layer). The framework of the Y zeolite is composed of cuboctahedral sodalite cages, themselves made up of Si, Al, and O atoms, which are intertwined tetrahedrally through O bridges to form hexagonal prisms and large cavities, the so-called supercages approximately 1.3 nm in diameter.[10−12,31−32] In each supercage, there are O-linked T atoms (Al or Si) 6- or 4-rings. Figure 1 shows the 6- and 4-rings and different sites in the supercages of the Y zeolites. [32] In our model, the second layer contains the O-linked T atoms (Al or Si) in the zeolite supercage as well as O and cap H atoms (see Figures 2 and 3). Geometry optimization was done with UB3LYP/6-31G(d,p) and the 6-ring or 4-ring at a lower level of theory, HF/STO-3G. The hyperfine coupling constants are computed in an ONIOM model of UB3LYP/ 6-311+G (2df,p): HF/STO-3G. The initial geometry of $Na^+$ (or $H^+$) and the second layer that consists of an O-linked 6-ring or 4-ring of T atoms was taken from the experimental data on the NaY zeolite by Fitch and co-workers.[31]

Vibrational frequencies are computed at the geometries of local minima. Binding energies between alkyl radicals and the zeolite host are also calculated from the energies necessary for removing the bound alkyl radicals.

**Results and Discussion**

**1. Geometries.** There are several sites that can be considered as the binding sites in both the NaY and HY zeolites. Each unit cell consists of eight sodalite cages and eight supercages (Figures 1, 3, and 4). The supercages are interconnected via circular windows that are formed by 12 T atoms and 12 O atoms and have a diameter of about 0.74 nm, large enough to grant access for small or medium molecules, such as methyl, ethyl, or *tert*-butyl. In comparison, only small molecules such as hydrogen can penetrate the largest 6-ring windows of the sodalite cages with a diameter of 0.22 nm. These sodalite windows are too narrow for even diatomic molecules, such as nitrogen or carbon monoxide, to pass through.[32,33] The T atoms in both the 6-ring and 4-ring are positioned in planes, while the O atoms are positioned above and below these planes, alternately in the direction of the inside or outside of the rings (Figure 1). There are four crystallographically distinct O atom sites: two of the framework O atoms (O1 and O4) are toward the supercage, while two others (O2 and O3) are mainly within the sodalite cages and the hexagonal prisms (Figure 3).

To model radicals in the NaY zeolite, we used six T atoms with a $Na^+$ at the ring center. This mimics the SII sites in the supercage of the NaY zeolite, known to be the preferred absorption site of ethene[33] (Figure 4). In the T-atom model, the charge on every T atom is determined by the average of the partial charges on Si and Al, which depend on the Si/Al ratio.[33] We used this T-atom model for the following three reasons: (1) it gives a very good physical picture for binding of ethene to the NaY zeolite;[33] (2) our investigations with explicit Al in the 6-rings always lead to the position of $Na^+$ close to the ring center; and (3) experimentally, the free radical signals will be averaged over all different possible substitution sites of Al in the 6-rings of the entire zeolite. This situation is on average equivalent to a symmetric T-atom model for the 6-ring.

Our models for adsorption of alkyl radicals in the HY zeolites include two possible sites for addition of ethene[34,35] (Figures 1, 3, and 5). Both models include Al in the ring explicitly (see Figure 3). It should be noted that ethene and isobutene do not fit in the sodalite cages and therefore the O1H and O4H sites are the only possible binding sites in the HY zeolite other than the window site, consistent with theoretical studies on the adsorption of ethene on the HY zeolite using ab initio methods.[34,35] The adsorption sites in both these studies are the crystallographically distinct O sites in the zeolite faujasite,[36] which mimic the O1H and O4H sites[34,36] (Figures 3 and 5).

For the sake of comparison with the T-atom model of the NaY zeolite, we also report the result of the T-atom calculations for the HY zeolite, where $H^+$ stays close to the center of the 6-ring. However, it should be emphasized that this model is *only* for comparison purposes, since our calculations show that $H^+$ always moves to the O4H site away from the center of the 6-ring with explicit Al and is quite different from $Na^+$ in the NaY zeolite, which always stays close to the center of the 6-ring.

The complexes we considered are $CH_3 \cdot Na^+$, $CH_3 \cdot H^+$, $C_2H_5 \cdot Na^+$, $C_2H_5 \cdot H^+$, $C(CH_3)_3 \cdot H^+$, $C(CH_3)_3 \cdot Na^+$, ethyl radicals on the 4-ring, and all alkyl radicals on 6-rings. Representative optimized structures are presented in Figures 2 and 3 and selected bond distances and angles are reported in Table 1. Our computational results agree well with the previous studies of Pacansky et al.[37] and Tachikawa et al.[38] on alkyl radicals. In the case of the methyl radical, both CH bond length and HCH bond angle agree perfectly with experimental data. [39]
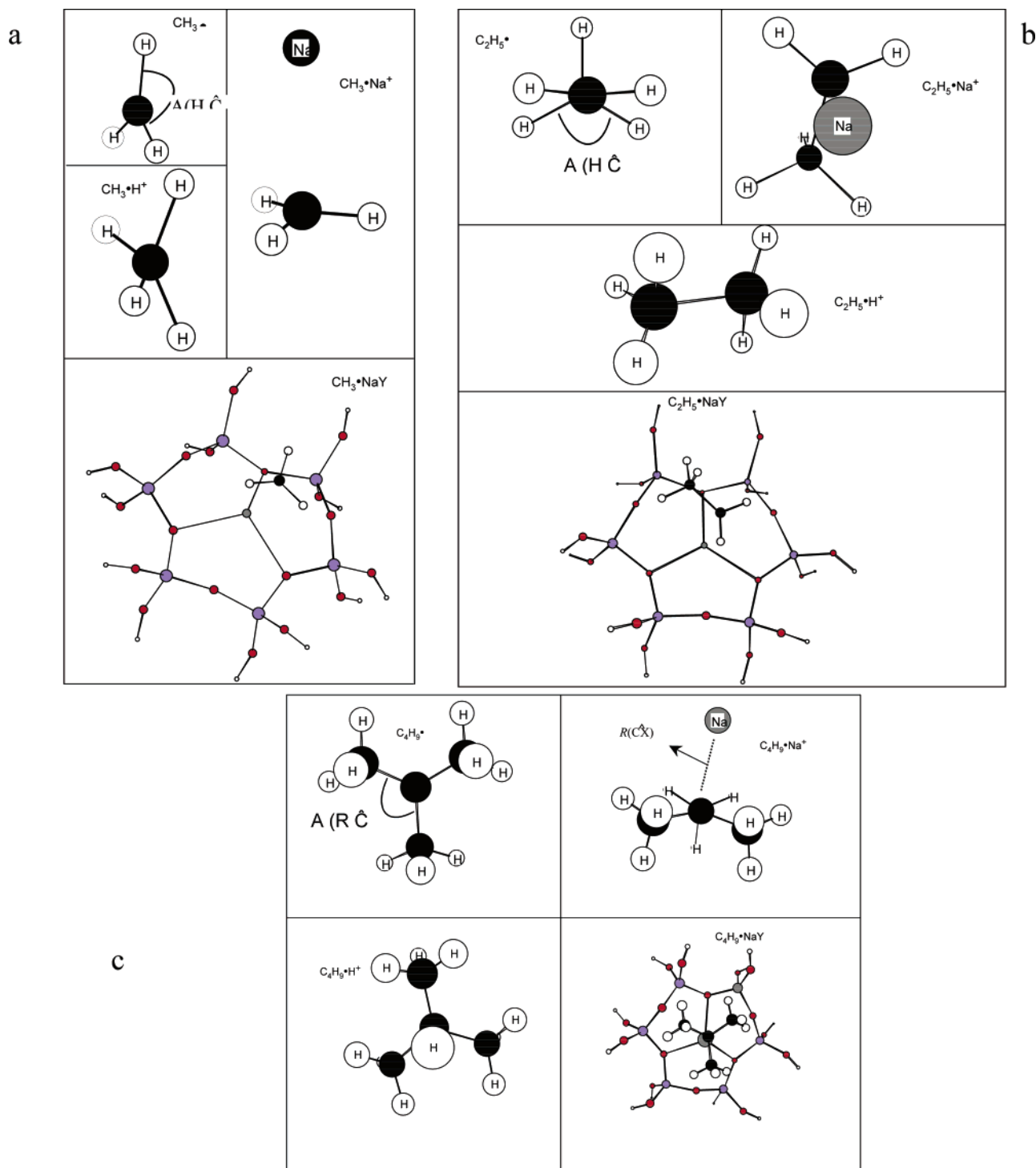
**Figure 2.** Optimized alkyl radical geometries in a vacuum and in complexes to free Na$^+$, free H$^+$, and Na$^+$ in a 6-ring of the NaY zeolite super cage: (a) methyl, (b) ethyl, and (c) *tert*-butyl radical. C atoms are presented with black spheres without labels; on the 6-ring, H atoms are presented with white spheres, Na$^+$ with gray spheres, T atoms with blue spheres, and O atoms with red spheres.

In comparison with the available experimental data,[13] preliminary studies indicate that the asymmetric substitution of Al in the 6-ring of the NaY zeolite leads to an unrealistic temperature dependence of the isotropic hfc. The asymmetric substitutions are either one or two Al substitutions with at least one Si atom in between. The geometries of alkyl radicals in the NaY zeolite reported in Table 1 are for the T-atom model, which has been reported to simulate ethene adsorption in the NaY zeolite very well.[33]

A general conclusion can be drawn from geometries in Figures 2 and 3: In both optimized ethyl and *tert*-butyl in the NaY

zeolites and in the case where Na$^+$ is replaced by H$^+$, the C—C bonds (where Ĉ is the C atom with the most unpaired electron density in Figures 2 and 3) are slightly tilted from a parallel geometry relative to the plane of the 6-ring, in which Na$^+$ or H$^+$ is close enough to bind two C atoms in these radicals. On the other hand, Figure 5 clearly shows that the ethyl radical on the O1H site in the HY zeolite is oriented differently, with the Ĉ—C bond almost vertical to the plane of the 4-ring. The ethyl radical at the O4H site is ca. 60° from the plane of the 6-ring.

For the carbon atom Ĉ with the largest unpaired electron density (the radical center), the angle $A(RĈR')$ in Table 1 is

Alkyl Radicals in Zeolites

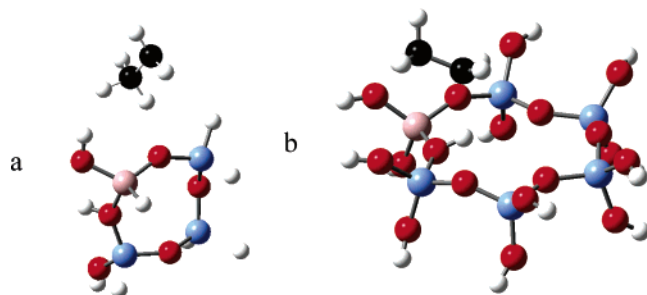*J. Phys. Chem. A, Vol. 109, No. 32, 2005* **7245**



**Figure 3.** Optimized ethyl radical geometry in the HY zeolite supercage (atom color schemes are the same as in Figure 2, except that Al is presented in pink). The left picture represents the binding at the O1H site and the right picture represents binding at the O4H site.
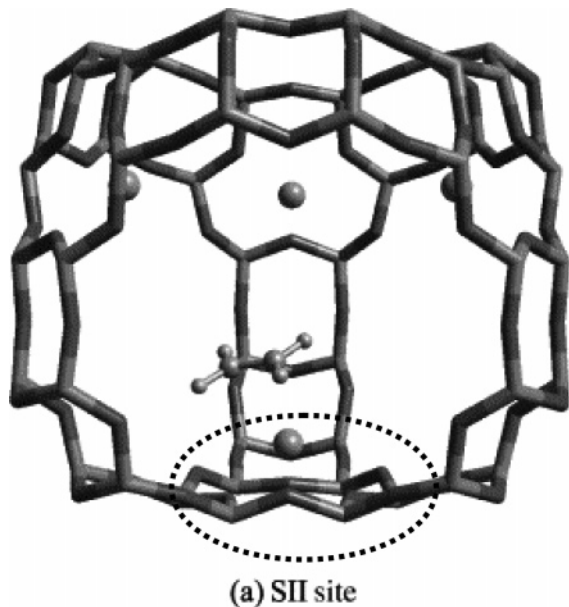


(a) SII site

**Figure 4.** The binding site of ethene in the NaY zeolite (adapted from ref 33 with permission). The dashed line circles the section selected for the modeling of the SII site in Figure 2.

the angle $A(H\hat{C}H)$ in the cases of methyl and ethyl radicals (see Figures 2 and 3) and is the angle $A(C\hat{C}C)$ in the case of the *tert*-butyl radical (Figure 2). If the angle $A(R\hat{C}R')$ is different from 120°, then the geometry deviates from planarity. The data in Table 1 show that, in all cases (except cationic complexes with $H^+$), the radicals are only slightly nonplanar at the radical center. However, the $H^+$ complexes give nonplanar equilibrium structures (except for the *tert*-butyl radical). The largest deviation from planar geometry of alkyl radical complexes to $Na^+$ and the NaY zeolite occurs for the ethyl radical.

Now, we consider the structural implications of binding between cations and alkyl radicals on bond lengths, which are important in determining the catalytic activity of alkyl radicals in the NaY and HY zeolites. For the methyl radical, cations are found to weaken the associated CH bonds, which are elongated by 0.007 Å in $CH_3 \cdot Na^+$ and $CH_3 \cdot NaY$, and by 0.04 Å in $CH_3 \cdot H^+$ and $CH_3 \cdot HY$ (T atom). This means that the effects of $H^+$ and $Na^+$ are in the same direction, but much more significant for $H^+$. However, when a more realistic model of the framework is taken into account, as in the case of $CH_3 \cdot HY$ (O1H and O4H), the effect is opposite, i.e., the CH bonds are strengthened. For the ethyl radical, $H^+$ is found to weaken the associated eclipse $\beta$ CH bond significantly and to strengthen the adjacent $\beta$ staggered CH bonds, which are shortened by 0.007 Å in $C_2H_5 \cdot H^+$ and $C_2H_5 \cdot HY$ (T atom). Again, in the case of the O4H site,

**TABLE 1: The CH Bond Distances (in Å) for Methyl Groups, $R^m(CH)_i$; the Distance (in Å) from Cation to the Radical Center C (the carbon atom with the most unpaired electron density) in the Free Radical, $R(\hat{C}X)$; and Angles, $A(R\hat{C}R')^a$**

| system | $R^m(CH)_1$ | $R^m(CH)_2$ | $A(R\hat{C}R')$ | $R(\hat{C}X)$ | $R(\hat{C}C)$ |
|---|---|---|---|---|---|
| $CH_3\cdot$ | 1.079 | | 120 | | |
| | 1.079[b] | | 120[b] | | |
| | 1.078[c] | | 120[c] | | |
| $CH_3\cdot Na^+$ | 1.087 | | 119 | 2.667 | |
| $CH_3\cdot H^+$ | 1.123 | | 97 | 1.123 | |
| $CH_3\cdot NaY$ | 1.085 | | 119 | 2.832 | |
| $CH_3\cdot HY$ (T atom) | 1.124 | | 97 | 1.092 | |
| $CH_3\cdot HY$ (O1H) | 1.047 | 1.052 | 115 | 2.426 | |
| $CH_3\cdot HY$ (O4H) | 1.045 | 1.049 | 116 | 2.407 | |
| $C_2H_5\cdot$ | 1.096 | 1.104 | 119 | | 1.489 |
| | 1.093[b] | 1.099[b] | 118[b] | | 1.492[b] |
| $C_2H_5\cdot Na^+$ | 1.095 | 1.105 | 116 | 2.612 | 1.489 |
| $C_2H_5\cdot H^+$ | 1.089 | 1.145 | 110 | 1.145 | 1.579 |
| $C_2H_5\cdot NaY$ | 1.096 | 1.105 | 116 | 2.616 | 1.490 |
| $C_2H_5\cdot HY$ (T atom) | 1.089 | 1.089 | 110 | 1.149 | 1.580 |
| $C_2H_5\cdot HY$ (O1H) | 1.092 | 1.110 | 114 | 3.821 | 1.475 |
| $C_2H_5\cdot HY$ (O4H) | 1.065 | 1.080 | 109 | 1.088 | 1.471 |
| $C(CH_3)_3\cdot$ | 1.096 | 1.106 | 119 | | 1.497 |
| | 1.094[b] | 1.102[b] | 118[b] | | |
| $C(CH_3)_3\cdot Na^+$ | 1.096 | 1.104 | 118 | 2.551 | 1.506 |
| $C(CH_3)_3\cdot H^+$ | 1.092 | 1.109 | 120 | 2.735 | 1.470 |
| $C(CH_3)_3\cdot NaY$ | 1.096 | 1.106 | 118 | 4.123 | 1.497 |
| $C(CH_3)_3\cdot HY$ (T atom) | 1.095 | 1.108 | 118 | 2.499 | 1.501 |
| $C(CH_3)_3\cdot HY$ (O1H) | 1.093 | 1.097 | 118 | 4.188 | 1.485 |
| $C(CH_3)_3\cdot HY$ (O4H) | 1.094 | 1.105 | 117 | 3.882 | 1.484 |

$^a$ $A(R\hat{C}R')$ will be the angle $A(H\hat{C}H)$ in the case of methyl and ethyl radicals and will be the angle $A(C\hat{C}C)$ angle in the case of the *tert*-butyl radical. $^b$ UMP2/6-311G** calculation results by Pacansky et al.[37] $^c$ QCISD calculation results of Tachikawa et al.[38]
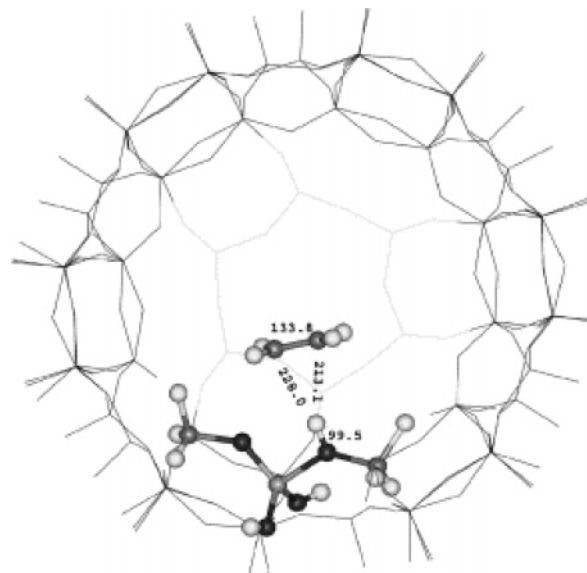


**Figure 5.** One of the binding sites of ethene in the HY zeolite and the cluster model used for calculations in ref 34. (Adapted from ref 34 with the permission.)

$H^+$ is found to strengthen the associated eclipse $\beta$ and staggered CH bonds, which are shortened by 0.02 and 0.03 Å, respectively. In the case of O1H, the associated eclipse $\beta$ CH bond is shortened while the staggered CH bond is elongated. $H^+$ strengthens the adjacent C−C bonds in the *tert*-butyl free radicals from binding to $H^+$ in the HY zeolite. $Na^+$ (either as a free cation or in the zeolite framework) is found to only weaken the CH bonds in methyl significantly.

Ghandi et al.

**TABLE 2: Average Binding Strengths (in kcal/mol) between Each Free Radical and Cation**

| system | binding strength | binding strength (with the ZPVE) |
|---|---|---|
| $CH_3 \cdot H^+$ | 132.89 | 129.12 |
| $CH_3 \cdot Na^+$ | 0.20 | −1.84 |
| $CH_3 \cdot NaY$ | 8.20 | |
| $CH_3 \cdot HY$ (O1H) | 1.26 | |
| $CH_3 \cdot HY$ (O4H) | 6.34 | |
| $CH_3 \cdot HY$ (T atom) | 17.01 | |
| $C_2H_5 \cdot H^+$ | 157.62 | 152.75 |
| $C_2H_5 \cdot Na^+$ | 15.18 | 13.91 |
| $C_2H_5 \cdot NaY$ | 32.74 | |
| $C_2H_5 \cdot HY$ (O1H) | 57.74 | |
| $C_2H_5 \cdot HY$ (O4H) | 78.12 | |
| $C_2H_5 \cdot HY$ (T atom) | 25.95 | |
| $C(CH_3)_3 \cdot Na^+$ | 17.23 | 16.53 |
| $C(CH_3)_3 \cdot H^+$ | 158.33 | 157.70 |
| $C(CH_3)_3 \cdot NaY$ | 6.47 | |
| $C(CH_3)_3 \cdot HY$ (O1H) | 78.48 | |
| $C(CH_3)_3 \cdot HY$ (O4H) | 80.72 | |
| $C(CH_3)_3 \cdot HY$ (T atom) | 47.97 | |

These effects clearly indicate that both the framework and the cation positions influence the structure of the adsorbed alkyl radicals. Since one of the catalytic functions of zeolites is to weaken CH bonds to increase their reactivity toward hydrogen abstraction, our finding helps to explain the catalytic activity of the zeolites and in particular their effects on the reactivity of the CH bonds in the alkyl radicals within the zeolites.

**2. Guest−Host Bond Characteristics.** Binding strength in a given complex is defined as the energy required to remove the bound species. Average binding strengths are shown in the first two columns of Table 2 for binding to cations or to the binding sites in zeolites (Figures 2−5). We considered the complexes with significant binding strengths (>100 kcal/mol) to be chemically bound, i.e., radical cation complexes.

Binding strengths of alkyl radicals to cations are similar in the case of $Na^+$ and the NaY zeolite; however, the existence of the zeolite framework does increase the free radical−$Na^+$ binding in the case of methyl and ethyl radicals and decrease it in the case of *tert*-butyl radical. The amplifying effect of framework on binding energies (by almost a factor of 2) is probably due to a combination of the effect of framework on the degree of charge transfer and on the hydrogen binding between H atoms of the free radical and the oxygen atoms of the zeolite framework. The steric effects of the bulky radical structure probably cause the decrease of binding strength for the *tert*-butyl radical. Finally, it should be noted that the binding energy of methyl is almost always smaller than those of the ethyl and *tert*-butyl free radicals in all sites, most probably due to the smaller dipole of methyl free radicals.

We have also calculated the binding strength of ethene to the NaY zeolite within the T-atom model for comparison and our result was 10 kcal/mol, in agreement with the theoretical result by Henson et al.,[33] who predicted the binding strength to be 9 kcal/mol. Upon the addition of the muonium to ethene, the binding strength increases by a factor of 3, reaching 32.74 kcal/mol (see Table 2).

In the second column of Table 2, we reported the zero-point vibrational energy (ZPVE) corrected binding strengths for free cation−free radical systems. The trend is similar in all cases, namely the ZPVE correction reduces the binding strength. Since there is a consistent trend in all cases, we assume the same would hold for free radicals to cations in the zeolite frameworks.
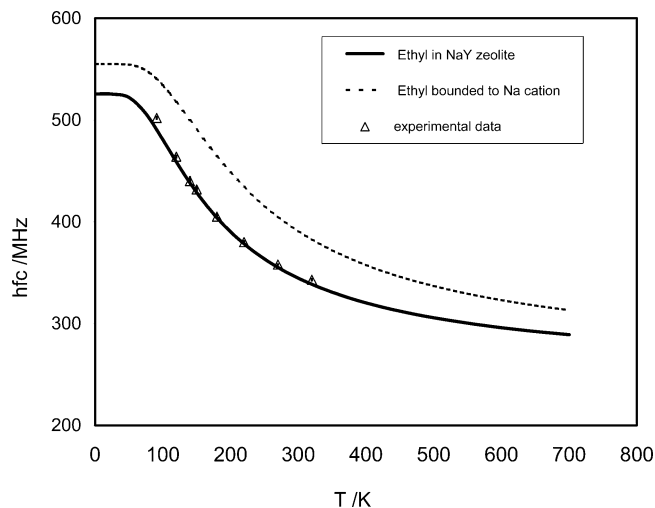


**Figure 6.** The experimental data for the temperature-dependent muon-electron hyperfine-coupling constants of the muoniated ethyl radical in the NaY zeolite (triangles) along with the theoretical data for the ethyl radical on free $Na^+$ (dashed line) and on $Na^+$ in the NaY zeolite super cage (thick line).
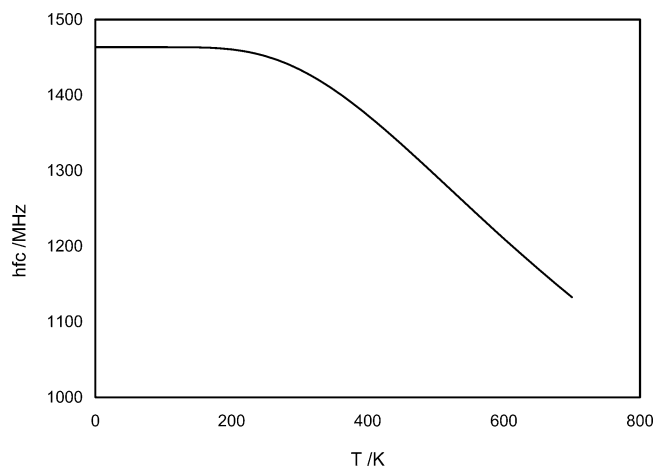


**Figure 7.** Theoretical predictions of the temperature-dependent muon-electron hyperfine-coupling constants for ethyl radical cation.

**3. Effect of Guest−Host Interactions on Hyperfine Interactions and Their Temperature Dependence for Ethyl Radicals.** The spin Hamiltonian for the electron spin ($S_e$) and the muon spin ($I_\mu$) has the form $S_e \cdot A \cdot I_\mu$, where $A$ is the hyperfine coupling tensor:

$$A = A_{iso} + D \qquad (1)$$

where $D$ stands for anisotropic hyperfine coupling tensor (dipolar interaction).

Figure 6 shows the experimental and theoretical temperature-dependent muon hfcs of ethyl radical in the NaY zeolite (will be described later). Figure 7 shows theoretical results for the ethane radical cation.

The temperature dependence of muon hfcs is usually described by the McConnell equation:[14,15,40−43]

$$A_{iso} = L + M\langle \cos^2 \theta \rangle \qquad (2)$$

where $L$ and $M$ are both assumed to be constants (independent of temperature) and proportional to the spin density at the C atom that muon is bound to, and the angle $\theta$ is defined in Figure 8. Comparison of the computed hfcs for the three H atoms in methyl groups with the experimental values at the lowest
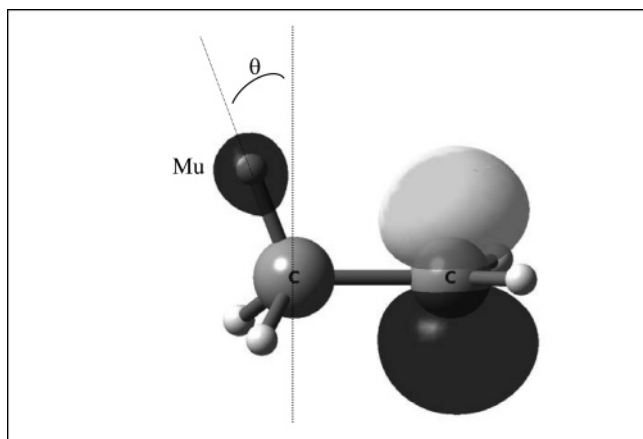
**Figure 8.** Schematic presentation of the dihedral angle between the C−Mu bond and the plane having the C−C bond and the single-occupied p orbital on the radical center $\hat{C}$. The square box signifies this plane.

temperature achieved experimentally suggests that muonium selectively occupies a position close to $\theta = 0^o$ (see Figure 8), parallel to the single-occupied p orbital on the radical center $\hat{C}$ in all cases.

The computed isotropic hfcs in Table 4 suggest that $Na^+$ and $H^+$ (either free or embedded in the zeolite framework) perturb the electronic wave functions of the free radicals significantly. For all free radicals, the perturbation by $Na^+$ causes significant delocalization of the spin density from the radical to the $Na^+$. However, the difference between the effect on the hfcs of the free $Na^+$ and the $Na^+$ within the zeolite framework bound to the free radical is only significant for methyl and *tert*-butyl radicals.

The computational results imply that Mu in the $CH_2Mu$ group takes a fixed position at temperatures below ~50 K (the onset of the plateau at low temperature in Figure 6), where muonium selectively occupies a position close to $\theta = 0°$ (see Figure 8), parallel to the unpaired p orbital on the radical center $\hat{C}$ in all cases.

The preference for Mu to occupy the $\theta \sim 0°$ position and the temperature dependence of muon hfcs can be qualitatively explained by hyperconjugation which is maximal around $\theta = 0°$ (see Figure 8).[43] Through this effect, the singly occupied molecular orbital will be delocalized between the radical center $\hat{C}$ and the adjacent CH $\sigma$ bond in the same plane, making the corresponding C−H bond weaker and longer. At 0 K, the total energy includes only the electronic energy and the ZPVE. Within the Born−Oppenheimer approximation, the electronic energy of Mu and H isotopomers is the same and therefore the ZPVE is the only factor that differentiates among different conformations at 0 K. Since the ZPVE of a C−H stretching vibration, to a first approximation, is proportional to $(k/m)^{1/2}$, where $k$ is the force constant and $m$ the mass of the hydrogen isotope, the increase in the ZPVE upon muoniation will be smaller for bonds with smaller force constants. The muonium atom thus occupies the site with the smaller force constant, i.e. the $\theta \sim 0°$ position. Similar effects have been reported for many neutral alkyl radicals before,[14,15,41−43] but not in zeolites.

If a free radical can exist in several rapidly interchanging conformers,[41−49] when the interchange rate is much larger than the difference between the associated hyperfine frequencies, a mean hfc will be obtained:

$$\langle A \rangle = \sum_i P_i A_i \qquad (3)$$

where $P_i$ is the probability of finding the $i$th conformer and $A_i$ is the corresponding hfc.

As already mentioned earlier, Mu will preferentially occupy sites with smaller C−H bond force constants, to minimize the ZPVE. One way to approach the temperature dependence of hfcs is to determine $A_i$ at each $i$ and vary *the conformation* in small increments, i.e., along the potential energy surface (PES) relevant to the hindered rotation. The next step will be to calculate rovibartional energy levels and wave functions for the particular states and use the Boltzmann distribution in eq 3 to compute the average hfc.[46,49] This scheme is computationally expensive due to the large number of atoms involved. So, for an approximation, we consider only the minimal energy conformations along the rotational PES. Different conformational minima along the rotational PES will have different ZPVE's depending on the position of Mu. At higher temperatures, such rotational conformers where Mu occupies less favorable sites will have appreciable probabilities. If the different rotational conformers are populated according to the Boltzmann distribution, a dependency on the temperature can be easily computed (see Figures 7 and 8). From the data on hyperfine interactions shown in Figures 7 and 8 and Table 4, we can draw several qualitative conclusions.

The hfcs of ethane radical cations are very large and weakly dependent on the temperature for temperatures below 300 K.

The *experimentally* observed free radical in ethene-loaded zeolites is not the free radical cation: the theoretical calculations suggest that the muoniated radical is a neutral ethyl radical as its isotropic muon hfc is much smaller than that of the computed free radical cation. However, this cannot rule out formation of the radical cations, but may suggest that the radical cations have been formed and have not been detected due to their extremely high values of isotropic hfcs. Efforts are underway to detect the radical cations, based upon our theoretical predictions.

The binding site for the ethyl radical is the 6-ring in the NaY zeolite, in particular the 6-ring with symmetric Al substitution (comparable to the T-atom model).

There is a clear deviation of the computed muon hfcs in the ethyl radical bound to $Na^+$ in the NaY zeolite and to free $Na^+$ at all temperatures (see Figure 6). The significant difference between the hfcs of $\hat{C}$ in the ethyl radical and $\hat{C}$ in the ethyl radical bound to $Na^+$ in the NaY zeolite and to free $Na^+$ suggests that the spin polarization of the free radical is strongly affected by its binding to the cation sites. In addition to the effect on the spin polarization of the free radical, the trend of muon hfcs is also consistent with the degree of charge transfers reported in Table 2. There is more charge transfer from the free radical to the NaY zeolite than to free $Na^+$, i.e., less electron density remained on the ethyl radical bound to $Na^+$ in the NaY zeolite than on the ethyl radical bound to free $Na^+$. It is evident from this example that the zeolite framework significantly affects the electronic structure of free radicals bound to the cation sites.

The agreement between our theoretical predictions and experimental data for $T > 100$ K gives us some confidence that our model remains reasonable at temperatures where experimental data are not available to compare. However, some caution is warranted for the following two reasons.

The typical time window (between ~1 and ~1000 ns) for detection of free radicals in zeolites by $\mu$SR techniques at low temperatures is short. If we consider the mechanism of radical formation through the addition of a thermal Mu to an alkene double bond,[14,15] the following sequence of events must occur in a $\mu$SR experiment:

**TABLE 3: Isotropic Hyperfine Coupling Constants (in MHz) at 0 K, Compared with Available Experimental Data at Low Temperatures in the Literature**

| system | Mu | H1 [$\beta$] | H2 [$\beta$] | H1 [$\alpha$] | H2 [$\alpha$] | $^{13}\hat{C}$ | $^{13}C$ | X |
|---|---|---|---|---|---|---|---|---|
| $CH_2Mu^\bullet$ | −178 | | | −60 | −60 | 74 | | |
| | −189[a] | | | −61[a] | −61[a] | 76[b] | | |
| $CH_2Mu \cdot Na^+$ | −122 | | | −41 | −41 | 65 | | 131 |
| $CH_2Mu \cdot H^+$ | 661 | | | 226 | 229 | 97 | | 219 |
| $CH_2Mu \cdot NaY$ | −127 | | | −43 | −43 | 63 | | 104 |
| $C_2H_4Mu^\bullet$ | 452 | 37 | 37 | −58 | −58 | 77 | −32 | |
| | 451[c] | | | | | 82[b] | −38[b] | |
| $C_2H_4Mu \cdot Na^+$ | 555 | 36 | 35 | −30 | −30 | 69 | −24 | 159 |
| $C_2H_4Mu \cdot H^+$ | 1463 | −18 | −18 | −18 | −18 | 14 | 14 | 437 |
| $C_2H_4Mu \cdot NaY$ | 526 | 37 | 38 | −33 | −33 | 67 | −26 | 156 |
| $C(CH_3)_2CH_2Mu^\bullet$ | 425 | 29 | 27 | | | 113 | −26 | |
| | 463[d] | | | | | | | |
| $C(CH_3)_2CH_2Mu \cdot Na^+$ | 417 | 26 | 26 | | | 122 | −13 | 103 |
| $C(CH_3)_2CH_2Mu \cdot H^+$ | 35 | 3 | 3 | | | 7 | 2 | 1301 |
| $C(CH_3)_2CH_2Mu \cdot NaY$ | 415 | 29 | 33 | | | 288 | −63 | 135 |

[a] Data from ref 40 in liquid ketene at 184 K. [b] Data from ref 41 on nonmuoniated methyl and ethyl radicals (0 K interpolation of the experimental data). [c] Data from ref 42 at 20 K. [d] Data from ref 43 at 43 K in solid isobutene.

**TABLE 4: The Experimental and Theoretical Anisotropic Splitting Constants (in G) for the Ethyl Radical, and Theoretical Anisotropic Splitting Constants (parallel to C−C bond components) for H, Mu, $^{13}$C, and X Nuclei of Muoniated Ethyl Radical**

| system | Mu | $\langle H_\beta \rangle$[a] | $^{13}\hat{C}$ | $^{13}C$ | X |
|---|---|---|---|---|---|
| $C_2H_5^\bullet$ (experiment)[44] | | 1.9 | | | |
| $C_2H_5^\bullet$ (experiment)[45] | | 2.4 | | | |
| $C_2H_5^\bullet$ (theory)[46] | | 2.5 | −27.2 | 0.5 | |
| $C_2H_4Mu^\bullet$ (at 0 K) | 2.7 | 2.7 | −27.3 | 0.6 | |
| $C_2H_4Mu \cdot Na^+$ (at 0 K) | 2.2 | 2.8 | −21.8 | 0.9 | 1.3 |
| $C_2H_5 \cdot HY$ (O4H) (at 0 K) | 7.6 | 1.5 | −0.4 | 0.5 | 0.1 |
| $C_2H_4Mu \cdot NaY$ (at 0 K) | 4.1 | 3.9 | −24.6 | 0.1 | 1.5 |
| $C_2H_4Mu \cdot H^+$ (at 0 K) | 6.3 | −5.1 | −15.0 | −15.0 | 6.3 |

[a] Average values of all $\beta$ hydrogen atoms. A similar averaging scheme was used in ref 46.

(1) The alkene (e.g., ethene) molecule is adsorbed at the minimum global energy site forming an alkene−zeolite complex, after the equilibration time, about half an hour, after a change of temperature before each subsequent experiment.

(2) A thermal Mu diffuses through the zeolite cages and finds its way to the adsorbed alkene molecules. This must happen in less than ∼100 ns in order for the formed free radical to be observable in transverse magnetic field. Diffusion of Mu happens in less than 100 ns, even at temperatures as low as 0.1 K, due to its significant tunneling effect.[14] Therefore, we can assume that under the entire temperature range of this study, Mu adds to the adsorbed alkene, which is resting at its *minimum energy geometry* position in the zeolite.

(3) The formed free radicals then move toward their ***global minimum energy geometry positions*** in the zeolite. This is a significantly temperature-dependent process. Such motions are practically frozen out at very low temperatures within the time window for TF-$\mu$SR. This means that although at higher temperatures the alkyl radical is mobile enough to find its minimum energy site, this may not be the case even after about 100 ns at very low temperatures. This factor should be taken into account when comparing the experimental data with the theoretical results. Moreover, in the computational model of the temperature dependence of hfcs, we assumed the equilibrium Boltzmann distribution, which is valid only if a free radical can exist in several rapidly interchanging conformers. Considering the significant binding of the alkyl radicals in zeolites (see Table

2), it is possible that such an assumption is invalid at very low temperatures, i.e. the system is far from the equilibrium within the time window of the experiment.

$\mu$SR experiments can provide information on both isotropic and anisotropic hfcs.[14b] The anisotropic hfcs for the ethyl radical are approximately axially symmetric about the CC bond,[44,45] i.e., the two components are $D_\perp$ and $D_\parallel = D_{zz}$.[14, 46−48]

The axial form of the hyperfine coupling tensor of the ethyl radical has been accounted for by rotation along the *CC* bond (z) axis (both intermolecular and intramolecular), which rapidly averages any *xy* anisotropy.[46] Our theoretical results as well as the previous theoretical[46,49] and experimental ESR results,[44,45] for the $\alpha$ and $\beta$ carbons of the ethyl radical and the ethyl radical bound to cations and zeolite framework, are reported in Table 4. These data, their temperature dependence, and the nature of anisotropic tensor are important for analyzing the $\mu$SR data.[9−12] The temperature dependence can be calculated in the same way as that of the isotropic hfcs.[13b]

**4. Vibrational Frequencies.** The most powerful tools for characterization of free radical vibrational motions are IR and resonance Raman spectroscopies. However, such experimental studies have never been performed for muoniated free radicals. A recent work advanced by one of the authors[50] is a promising step in this direction. Since these experimental studies are very demanding, precise computational studies of vibrational frequencies and intensities are required before designing such experiments. The reasonable agreement between our theoretical results and the experimental data (see Figure 6) prompted us to report the effect of cations on the vibrational frequencies and intensity of light absorption for muoniated free radicals.

First (supporting material), we evaluated our method by comparing our calculations of methyl frequencies with the experimental data[51] and the computational results of Pacansky et al.[37] The overall agreement between experimental and our calculated frequencies is better than that with the results of Pacansky et al.[37] Comparison of our computational results with MP2 results (see Table 5) confirms the general fact that the hybrid DFT gives a better picture of IR spectra than MP2 does.[52]

For low-frequency modes, mixing with the zeolite framework motions is probable, and size effects should be studied in detail to include the other parts of the supercage or even cations outside the super cage. Such studies are in progress and the results will be reported later. High-frequency C−Mu and C−C stretching modes are reported in Table 5.

Alkyl Radicals in Zeolites

*J. Phys. Chem. A, Vol. 109, No. 32, 2005* **7249**

**TABLE 5: The Ĉ−C Stretching and C−Mu Stretching Vibrational Frequencies (in cm$^{-1}$) and IR Intensities (in km/mol) for C−Mu Stretching Vibrational Modes**

| system | C−Mu stretching | C−Mu IR intensity | Ĉ−C stretching |
|---|---|---|---|
| CH$_2$Mu$^•$ | 9412 | 42 | |
| CH$_2$Mu·H$^+$ | 8222 | 1975 | |
| CH$_2$Mu·Na$^+$ | 9291 | 13 | |
| CH$_2$Mu·NaY | 9178 | 5 | |
| C$_2$H$_4$Mu$^•$ | 8914 | 230 | 1096 |
| C$_2$H$_4$Mu·H$^+$ | 9233 | 173 | 463 |
| C$_2$H$_4$Mu·Na$^+$ | 8970 | 47 | 1045 |
| C$_2$H$_4$Mu·NaY | 8647 | 109 | 1064 |
| C(CH$_3$)$_2$CH$_2$Mu$^•$ | 8853 | 281 | 765 |
| C(CH$_3$)$_2$CH$_2$Mu·H$^+$ | 9085 | 33 | 811 |
| C(CH$_3$)$_2$CH$_2$Mu·Na$^+$ | 8663 | 6 | 763 |
| C(CH$_3$)$_2$CH$_2$Mu·NaY | 9196 | 106 | 710 |

The results in Table 5 suggest that the C−Mu stretches should be between 8000 and 9500 cm$^{-1}$, which is in a reasonable range for studies by conventional tuneable lasers, a unique aspect of muoniated free radicals as compared to their conventional isotopomers. While the C−Mu stretching modes are not mixed with any other modes, the C−C stretching modes have significant components of rocking, wagging, and umbrella motions. With these facts in mind, we can utilize the frequencies in Table 5 to obtain a qualitative picture of the effect of cations on C−Mu and C−C bonds.

From the order of the vibrational frequencies of the C−Mu stretching mode, we can see that the strength of the C−Mu bond in free radicals increases in the following order: *tert*-butyl < ethyl < methyl. The same order holds for complexes of the free radicals to Na$^+$. For the alkane radical cations, this order is broken and changed to methyl < *tert*-butyl < ethyl.

The Ĉ−C bond in muoniated ethyl is the strongest bond among these three alkyl radicals. The effect of H$^+$ on the Ĉ−C bond of the ethyl radical is quite significant and suggests that the Ĉ−C bond is very reactive in the ethane radical cation. This effect is reversed for the *tert*-butyl radical. In both free radicals, Na$^+$ has only minor weakening effects. These results from vibrational frequencies are consistent with the results on the structures of free radicals explained above. For the methyl radical, both H$^+$ and Na$^+$ cations are weakening the C−Mu bond. The zeolite framework has a further weakening effect probably due to the hydrogen bonding between Mu in C−Mu and O in the zeolite framework.

The highest intensity absorption is for C−Mu asymmetry stretching in the muoniated methane radical cation, followed by similar modes in neutral muoniated *tert*-butyl and ethyl radicals.

**5. Computational Predictions To Guide Future Experimental Studies.** Here, we report conditions needed to observe methyl radicals in the NaY and HY zeolites and to observe radical cations in the HY zeolite. All equations relevant to this section are given in the refs 12, 14, and 53.

At low temperatures diffusional motion of the free radicals is slow. As a rough estimate for the diffusion coefficient of alkyl radicals in the zeolites, we use the binding strength of an alkyl radical to the zeolite as a measure of the diffusion barrier. Using ethene as a standard,[54,55] where both its diffusion coefficient and binding strength in a zeolite are known, we estimate the diffusion coefficient of the alkyl radical according to the following formula:

$$D_{alkyl} = D_{St}e^{-BE/RT}/e^{-BE_{St}/RT_{St}} \qquad (4)$$

The diffusion coefficient of ethene ($D_{St}$) at 298 K ($T_{St}$) is 3.2

$\times$ 10$^{-10}$ m$^2$ s$^{-1}$,[54] while its binding strength to the NaY zeolite ($BE_{St}$) is 9 kcal/mol.[55] The binding of methyl radical to free Na$^+$ or Na$^+$ within the zeolite framework is small and therefore we expect that at a temperatures around 150 K, $D_{methyl}$ is about 1.5 $\times$ 10$^{-15}$ m$^2$ s$^{-1}$, corresponding to a mean square net displacement around 1 Å in 1 ms. Based on our computational results and a recent report on magnetic field dependence of $\mu$SR amplitudes,[53] we recommend the following conditions for detection of neutral muoniated methyl radical in HY or NaY zeolites, assuming a pseudo-first-order rate of 10$^9$ s$^{-1}$ for radical formation and assuming thermal reaction of Mu as the mechanism of radical formation: transverse field around 8000 G, where $v_{14}$ and $v_{23}$ would be the observable frequencies at 174 and 44 MHz, respectively, well separated from diamagnetic muon precession frequency ($v_d$) at 108.4 MHz.

Moreover, in view of significant recent developments in the production of $\alpha$ muoniated radicals,[40,56] and the unique characteristics of binding of methyl radicals in zeolites (see Table 2), we strongly recommend pursuing experimental studies of muoniated methyl radicals in zeolites.

To be able to detect methane radical cations, the best condition is at ~6000 G, where the two observable frequencies are $v_{12}$ = 243 MHz and $v_{34}$ = 418 MHz, with $v_d$ ~ 81 MHz. On the other hand, it would be difficult to detect the ethane radical cation within the current technical limits of TF-$\mu$SR, due to its very large muon hfc (see Table 4 and Figure 10).

*tert*-Butyl radical at ~400 K will have a hfc about 391.5 MHz. Assuming 10$^{10}$ s$^{-1}$ for the pseudo-first-order rate of radical formation under these conditions, the best condition will be at 10 000 G, where $v_{12}$ = 59 MHz, $v_{34}$ = 333 MHz, and $v_d$ = 135.5 MHz are the observable signals.

Isobutane radical cation in the HY zeolite would have a hfc about 30 MHz over the whole range of experimentally possible conditions. Due to the small hyperfine coupling, the two observable frequencies $v_{12}$ and $v_{34}$ will be very close to $v_d$ and will be difficult to observe, particularly when the *diamagnetic* signal is rather broad in these zeolites. At 4000 G, $v_{12}$ = 39 MHz and $v_{34}$ = 69 MHz, while $v_d$ = 54 MHz. A better way to search for isobutane radical cation might be by means of ALC-$\mu$SR.[14] The $\Delta M$ = 1 resonance of isobutane radical cation will be between 1100 and 1300 G at different temperatures, which is expected to be the only observable resonance due to large binding energy (see Table 2).

There should be other $\Delta M$ = 0 resonances for all free radicals in the NaY zeolite, due to the sodium ($I = ^3/_2$) nuclear hyperfine couplings (i.e., k stands for Na). Such resonances have been observed in $\mu$SR studies of Cu- and Na-exchanged ZSM-5 zeolites.[10,56] For ethyl in the NaY zeolite at a temperature around 100 K, it should give rise to a broad and strong resonance around 13 700 G, while near 0 K, it should give rise to a very broad resonance around 15 800 G.

**Conclusions**

We classified the free radicals that could form in the NaY and The HY zeolites from addition of muonium to ethene and isobutene. Geometries, binding energies, and temperature dependences of the hyperfine splitting in neutral methyl, ethyl, and *tert*-butyl radicals and their radical cations have been studied. The muon hyperfine coupling constants of ethane radical cations in the HY zeolite are very large with weak temperature dependence below 300 K. There is a significant binding between the ethyl or *tert*-butyl radical and the NaY or HY zeolite, but the *intramolecular* dynamics of these free radicals are only *weakly affected* by this binding. The binding of the NaY and

HY zeolites to both ethyl and *tert*-butyl radicals has a *significant effect* on their *intermolecular* dynamics, trapping these radicals on cation sites in zeolite super cages. The methyl radical in the NaY zeolite is predicted to be mobile due to its very small binding strength to the Na$^+$ cation sites.

**Supporting Information Available:** Table of experimental vibrational frequencies and their corresponding theoretical predictions for the methyl radical. This material is available free of charge via the Internet at http://pubs.acs.org.

## References and Notes

(1) Venuto, P. B. In *Progress in Zeolites and Microprous Materials*; Chon, H., Ed.; Elsevier: Amsterdam, The Netherlands, 1977.

(2) Vanden Berg, J. P.; Van Hoof, J. H. C. In *Proceedings of the 5th Conference on Zeolites*; Rees, L. V. C., Ed.; Heden: London, 1980.

(3) Bandiera, J.; ben Taarit, Y. *Appl. Catal.* **1991**, *76*, 199−208.

(4) Kutana, A.; Makarenko, B.; Rabalais, J. W. *J. Chem. Phys.* **2003**, *119*, 11906−11911.

(5) Somorjai, G. *Introduction to Surface Chemistry and Catalysis*; Wiley: New York, 1994.

(6) Lange, J. P.; Gutsze, A.; Karge, H. G. *J. Catal.* **1988**, *114*, 136−143.

(7) Hill, J.-R.; Freeman, C. M.; Delley, B. *J. Phys. Chem. A* **1999**, *103*, 3772−3777.

(8) Werst, D. W.; Choure, S. C.; Vinokur, E. I.; Xu, L. Q.; Trifunac, A. D. *J. Phys. Chem. B* **1999**, *103*, 9219−9230.

(9) Shelley, M.; Arseneau, D. J.; Senba, M.; Pan, J. J.; Snooks, R.; Kreitzman, S. R.; Fleming, D. G.; Roduner, E. In *Studies in Surface Science and Catalysis*; Wert Kamp, J., Ed., Elsevier: Amsterdam, The Netherlands, 1994.

(10) (a) Stolmár, M.; Roduner, E. *J. Am. Chem. Soc.* **1998**, *120*, 583−584. (b) Roduner, E.; Stolmár, M.; Dilger, H.; Reid, I. D. *J. Phys. Chem.* **1998**, *102*, 7591−7597.

(11) Beck, B.; Roduner, E.; Dilger, H.; Czarnecki, P.; Fleming, D. G.; Reid, I. D.; Rhodes, C. J. *Phys. B* **2000**, *289*, 607−611.

(12) (a) Fleming, D. G.; Shelley, M.; Arseneau, D. J.; Senba, M.; Pan, J. J.; Kreitzman, S. R.; Roduner, E. *Phys. B* **2000**, *289*, 603−606. (b) Fleming, D. G.; Shelley, M.; Arseneau, D. J.; Senba, M.; Pan, J. J.; Roduner, E. *J. Phys. Chem. B* **2002**, *106*, 6395−6407.

(13) (a) Fleming, D. G. *TRIUMF annual report for experiment 939*, 2003. (b) Bridges, M. D.; Ghandi, K.; Arseneau, D. J.; Fleming, D. G. *J. Phys. Chem. B*. In preparation.

(14) (a) Roduner, E.; Strub, W.; Burkhard, P.; Hochmann, J.; Percival, P. W.; Fisher, H.; Ramos, M.; Webster, B. C. *Chem. Phys.* **1982**, 67, 275. (b) Roduner, E. *Chem. Soc. Rev.* **1993**, *22*, 337−346.

(15) Yu, D.; Percival, P. W.; Brodovitch, J.-C.; Leung, S. K.; Kiefl, R. F.; Venkateswaran, K.; Cox, S. F. J. *Chem. Phys.* **1990**, *142*, 229−236.

(16) Fessenden, R. W.; Schuler, R. H. *J. Chem. Phys.* **1973**, *56*, 1575.

(17) Paul, H.; Fischer, H. *Helv. Chim. Acta* **1973**, *56*, 1575.

(18) Frisch, M. J.; Trucks, G. W.; Schlegel, H. B.; Scuseria, G. E.; Robb, M. A.; Cheeseman, J. R.; Zakrzewski, V. G.; Montgomery, J. A.; Stratmann, R. E.; Burant, J. C.; Dapprich, S.; Millam, J. M.; Daniels, A. D.; Kudin, K. N.; Strain, M. C.; Farkas, O.; Tomasi, J.; Barone, V.; Cossi, M.; Cammi, R.; Mennucci, B.; Pomelli, C.; Adamo, C.; Clifford, S.; Ochterski, J.; Petersson, G. A.; Ayala, P. Y.; Cui, Q.; Morokuma, K.; Malick, D. K.; Rabuck, A. D.; Raghavachari, K.; Foresman, J. B.; Cioslowski, J.; Ortiz, J. V.; Stefanov, B. B.; Liu, G.; Liashenko, A.; Piskorz, P.; Komaromi, I.; Gomperts, R.; Martin, R. L.; Fox, D. J.; Keith, T.; Al-Laham, M. A.; Peng, C. Y.; Nanayakkara, A.; Gonzalez, C.; Challacombe, M.; Gill, P. M. W.; Johnson, B. G.; Chen, W.; Wong, M. W.; Andres, J. L.; Head-Gordon, M.; Replogle, E. S.; Pople, J. A. *Gaussian 98*; Gaussian, Inc.: Pittsburgh, PA, 1998.

(19) Cohen, M. J.; Chong, D. P. *Chem. Phys. Lett.* **1995**, *234*, 405−412.

(20) Becke, A. D. *J. Chem. Phys.* **1993**, *98*, 5648−5652.

(21) Lee, C.; Yang, W.; Parr, R. G. *Phys. Rev. B* **1988**, *37*, 785−789.

(22) Barone, V. In *Recent Advances in Density Functional Methods*; Chong, D. P., Ed.; World Scientific: Singapore, 1995.

(23) Stephens, P. J.; Devlin, F. J.; Chabalowski, C. F.; Frisch, M. J. *J. Phys. Chem.* **1994**, *98*, 11623.

(24) (a) Wetmore, S. D.; Boyd, R. J.; Eriksson, A. L. *J. Chem. Phys.* **1997**, *106*, 7738−7748. (b) Lunell, S.; Eriksson, A. L.; Worstbrock, L. *J. Am. Chem. Soc.* **1991**, *113*, 7508−7512. Lunell, S.; Eriksson, A. L.; Worstbrock, L. *THEOCHEM* **1999**, *461*, 1−21.

(25) Maseras, F.; Morokuma, K. *J. Comput. Chem.* **1995**, *16*, 1170.

(26) Humbel, S.; Sieber, S.; Morokuma, K. *J. Chem. Phys.* **1959**−**1996**, *105*.

(27) Matsubara, T.; Sieber, S.; Morokuma, K. *Int. J. Quantum Chem.* **1996**, *60*, 1101.

(28) Svensson, M.; Humbel, S.; Froese, R. D. J.; Matsubara, T.; Sieber, S.; K. Morokuma, J. *Phys. Chem.* **1996**, *100*, 19357.

(29) Dapprich, S.; Komáromi, I.; Byun, K. S.; Morokuma, K.; Frisch, M. J. *J. Mol. Struct.* (*THEOCHEM*) **1999**, *462*, 1.

(30) Vreven, T.; Morokuma, K. *J. Comput. Chem.* **2000**, *21*, 1419.

(31) Fitch, A. N.; Jobic, H.; Renouprez, A. *J. Phys. Chem.* **1986**, *90*, 1311−1318.

(32) Hübnera, G.; Rauhutb, G.; Stollb, H.; Roduner, E. *Phys. Chem. Chem. Phys.* **2002**, *13*, 3112−3121.

(33) Henson, N. J.; Eckert, J.; Hay, P. J.; Redondo, A. *Chem. Phys.* **2000**, *261*, 111−124.

(34) Limtrakul, J.; Nanok, T.; Jungsuttiwong, S.; Khongpracha, P.; Truong, T. N. *Chem. Phys. Lett.* **2001**, *349*, 161−166.

(35) Evleth, E. M.; Kassab, E.; Jessri, H.; Allavena, M.; Montero, L.; Sierra, L. R. *J. Phys. Chem.* **1996**, *100*, 11368−11374.

(36) Hill, J.-R.; Freeman, C. M.; Delley, B. *J. Phys. Chem. A* **1999**, *103*, 3772−3777

(37) Pacansky, J.; Koch, W.; Miller, M. D. *J. Am. Chem. Soc.* **1991**, *113*, 317−328.

(38) Tachikawa, H.; Igarashi, M.; Ishibashi, T. *Chem. Phys. Lett.* **2002**, *352*, 113−119.

(39) Herzberg, G. *Electronic spectra and electronic structure of polyatomic molecules*; Van Nostrand: New York, 1966.

(40) McKenzie, I.; Addison-Jones, B.; Brodovitch, J.-C.; Ghandi, K.; Kecman, S.; Percival, P. W. *J. Phys. Chem.* **2002**, *106*, 7083−7085.

(41) Perera, S. A.; Salemi, L. M.; Bartlett, R. J. *J. Chem. Phys.* **1997**, *106*, 4061−4066.

(42) Percival, P. W.; Brodovitch, J.-C.; Leung, S. K.; Yu, D.; Kiefl, R. F.; Garner, D. M.; Arseneau, D. J.; Fleming, D. G.; Gonzalez, A.; Kempton, J. R.; Senba, M.; Venkateswaran, K.; Cox, S. F. J. *Chem. Phys. Lett.* **1989**, *163*, 241−245.

(43) (a) Percival, P. W.; Brodovitch, J.-C.; Leung, S. K.; Yu, D.; Kiefl, R. F.; Luke, G. M.; Venkateswaran, K.; Cox, S. F. J. *Chem. Phys.* **1988**, *127*, 137−141. (b) Komaguchi, K.; Marutani, T.; Shiotani, M.; Hasegawa, A. *Phys. Chem. Chem. Phys.* **2001**, *3*, 3536−3540. (c) Liu, W.; Lund, A.; Shiotani, M.; Michalik, J.; Biglino, D.; Bonora, M. *Appl. Magn. Reson.* **2003**, *24*, 285−302.

(44) McDowell, C. A.; Raghunthan, P.; Shimokoshi, K. *J. Chem. Phys.* **1973**, *58*, 114.

(45) Toriyama, K.; Iwasaki, M.; Nunome, K.; Muto, H. *J. Chem. Phys.* **1981**, *75*, 1633.

(46) Chipman, D. M. *J. Chem. Phys.* **1991**, *94*, 6632.

(47) Atherton, N. M. *Principles Of Electron Spin Resonance*; Prentice Hall: Upper Saddle River, NJ, 1993.

(48) Weltner, W. *Magnetic Atoms and Molecules*; Dover: New York, 1989.

(49) Suter, H. U.; Ha, T-K. *Chem. Phys.* **1991**, *154*, 227−236.

(50) Ghandi, K. Rutherford Appleton Laboratory Experimental Report, 2003, RB 14830.

(51) (a) Pacansky, J.; Waltman, R. J.; Barnes, L. A. *J. Phys. Chem.* **1996**, *100*, 16828−16834. (b) Pacansky, J.; Bargon, J. *J. Phys. Chem.* **1993**, *97*, 10694−10701. (c) Pacansky, J.; Dupuis, M. *J. Phys. Chem.* **1986**, *90*, 1980−1983. (d) Pacansky, J.; Coufal, H. *J. Chem. Phys.* **1980**, *72*, 3298−3304.

(52) (a) Barone, V.; Minichino, C.; Faucher, H.; Subra, R.; Grand, A. *Chem. Phys. Lett.* **1993**, *205*, 324−330. (b) Barone, V.; Minichino, C.; Grand, A.; Subra, R. *J. Chem. Phys.* **1993**, *99*, 6787−6798.

(53) Percival, P. W.; Brodovitch, J.-C.; Arseneau, D. J.; Senba, M.; Fleming, D. G. *Phys. B* **2003**, *326*, 72−75.

(54) Nivarthi, S. S.; Davis, H. T.; Mccormick, A. V. *Chem. Eng. Sci.* **1995**, *50*, 3217−3229.

(55) Choudary, V. R.; Mayadevi, S.; Singh, A. P. *J. Chem. Soc., Faraday Trans.* **1995**, *91*, 2935−2944.

(56) McKenzie, I.; Brodovitch, J.-C.; Ghandi, K.; Kecman, S.; Percival, P. W. *Phys. B* **2003**, *326*, 76−80.

(57) Roduner, E.; Solmar, M.; Dilger, H.; Himmer, U.; Shelley, M.; Reid, I. D. *Hyp. Int.* **1997**, *106*, 51−54.